Journal of Computational Physics 242 (2013) 869–888

Contents lists available at SciVerse ScienceDirect

Journal of Computational Physics

journal homepage: www.elsevier.com/locate/jcp

PIROCK: A swiss-knife partitioned implicit–explicit orthogonal Runge–Kutta Chebyshev integrator for stiff diffusion–advection–reaction problems with or without noise

Assyr Abdulle [a,*], Gilles Vilmart [b]

[a] Mathematics Section, École Polytechnique Fédérale de Lausanne, Station 8, 1015 Lausanne, Switzerland
[b] École Normale Supérieure de Cachan, Antenne de Bretagne, INRIA Rennes, IRMAR, CNRS, UEB, Av. Robert Schuman, F-35170 Bruz, France

ARTICLE INFO

Article history:
Received 11 October 2012
Received in revised form 16 January 2013
Accepted 5 February 2013
Available online 5 March 2013

Keywords:
ROCK method
Stabilized second-order integration method
Partitioned Runge–Kutta methods
Stiff problems
Advection–diffusion–reaction problems
Stochastic problems

ABSTRACT

A partitioned implicit–explicit orthogonal Runge–Kutta method (PIROCK) is proposed for the time integration of diffusion–advection–reaction problems with possibly severely stiff reaction terms and stiff stochastic terms. The diffusion terms are solved by the explicit second order orthogonal Chebyshev method (ROCK2), while the stiff reaction terms (solved implicitly) and the advection and noise terms (solved explicitly) are integrated in the algorithm as finishing procedures. It is shown that the various coupling (between diffusion, reaction, advection and noise) can be stabilized in the PIROCK method. The method, implemented in a single black-box code that is fully adaptive, provides error estimators for the various terms present in the problem, and requires from the user solely the right-hand side of the differential equation. Numerical experiments and comparisons with existing Chebyshev methods, IMEX methods and partitioned methods show the efficiency and flexibility of our new algorithm.

1. Introduction

We consider systems of ordinary differential equations (ODEs) representing space discretizations of PDEs of the form[1]

$$\dot{y} = F(y) = F_D(y) + F_A(y) + F_R(y), \quad y(0) = y_0, \tag{1}$$

where $F_D(y), F_A(y), F_R(y) \in \mathbb{R}^n$ represent diffusion terms with eigenvalues close to the negative real axis, advection terms with eigenvalues close to the imaginary axis, and stiff reaction terms, respectively. Assuming that (1) comes from a spatial discretization of an advection–diffusion–reaction problem in spatial dimension N and considering a spatial grid size Δx that leads to a system of ODEs of size $n = \mathcal{O}((\Delta x)^{-N})$, then the eigenvalues of the Jacobian of F_D are typically distributed along the negative real axis in an interval that grows as $[-\mathcal{O}((\Delta x)^{-2}), 0]$ (for a symmetric diffusion operator), the eigenvalues of F_A are typically distributed on the imaginary axis in an interval that grows as $[-i\mathcal{O}((\Delta x)^{-1}), i\mathcal{O}((\Delta x)^{-1})], i = \sqrt{-1}$, while the eigenvalues of the Jacobian of the reaction term F_R are usually not related to Δx but have a ratio (sometime called the stiffness ratio) $\max_j|\Re\lambda_j|/\min_j|\Re\lambda_j|$ that can be very large or vary over several orders of magnitude. The question of stability is central when applying an ODE solver to (1) and it is well known that explicit solvers usually face step size restriction for such problems (usually called stiff), essentially due to the terms F_D and F_R [1]. Implicit methods have usually no such

* Corresponding author. Tel.: +41 21 693 03 11.
E-mail addresses: Assyr.Abdulle@epfl.ch (A. Abdulle), Gilles.Vilmart@bretagne.ens-cachan.fr (G. Vilmart).

[1] An autonomous form is considered here for simplicity. We emphasize that our method is valid for a non-autonomous form as well.

0021-9991/$ - see front matter © 2013 Elsevier Inc. All rights reserved.
http://dx.doi.org/10.1016/j.jcp.2013.02.009

restriction but come at the cost of solving a large nonlinear system at each time step. For such nonlinear systems, iterative methods that are preferably used can become quite involved, particularly when the system has a complicated nonlinear structure [2].

Alternatives to fully implicit solvers have been proposed in the past. First, for problems involving only F_D, explicit stabilized Runge–Kutta (RK) methods have been developed [3–7]. These methods considerably reduce the cost of standard explicit methods by allowing for much larger time steps, thanks to a special stabilization procedure (involving shifted Chebyshev-like polynomials), obtained by increasing the internal stages s of the RK method. As the stability domains grow quadratically with s (also a measure of the numerical work in terms of function evaluations) along the negative real axis, this procedure is much more efficient than taking s steps of a standard explicit method (for which the stability domain would only grow linearly with the number of function evaluations). These methods are much easier to implement and to use than implicit solvers and can usually just be substituted into an explicit Euler procedure. They have also been shown to be competitive with implicit solvers for some classes of problems. This is illustrated in [8,5,6] with reaction–diffusion problems and in [2] for a combustion problems. In general, when the spatial discretization leads to a problem that prevents the use of direct solver for implicit methods (e.g., (sparse) LU), the efficiency of implicit solvers will be *problem dependent* and rely on the efficiency of appropriate iterative methods, good pre conditioners. Furthermore, efficient parallelization of the linear algebra arising from implicit solvers is a non trivial task, while it is straightforward for explicit solvers. Stabilized methods can also accommodate an advection term F_A, but remain efficient provided that the diffusion is dominant (small Peclet number regime). Moderate reaction terms F_R can also be integrated with such methods.

However, when the reaction term becomes very stiff or in the large Peclet number regime, classical explicit stabilized methods are no longer attractive. They can still be used to integrate part of the Eq. (1) in a splitting strategy. In presence of very stiff reactions, integrating the diffusion term with a stabilized method and the reaction term with an implicit method can be efficient [9]. Indeed, as the reaction term alone has no spatial connectivity, the nonlinear system for the reaction term can be decomposed in small independent systems that can be solved efficiently (e.g. with an LU decomposition). However, time step control and error estimates can be delicate with splitting methods. Due to the splitting error, the method proposed in [9] has second order even though each individual integrator used in the splitting strategy has a higher order. Another strategy based on partitioned RK methods (using the stabilized RKC method for the diffusion terms) has become popular. We mention the development of the implicit–explicit solver IRKC [10], a modification [11] as a two-step method with improved imaginary stability, and the partitioned method PRKC [12]. We notice that the PRKC method [12] is of second order, while the IRKC method [10] is formally of first order (due to the implicit Euler solver used for the reaction term), but with a global error constant that scales as $\mathcal{O}(h^2 + h/s^2)$ where s is the number of internal stages. The IRKC method is intended for problems of the type (1) with possibly stiff reactions treated implicitly, while the PRKC method is intended for problems of the type (1) with a *non-stiff* reaction term F_R which is potentially expensive to evaluate (the F_D and F_R terms are then integrated by different explicit methods). Finally, generalizations of stabilized methods for problems (1) that also include white noise have recently been proposed [13–15].

In this paper we introduce a new partitioned implicit–explicit integrator, called PIROCK, based on the explicit second order orthogonal Runge–Kutta–Chebyshev method (ROCK2) introduced in [5] and combining ideas from [7,14,15,12]. We derive a single algorithm that can combine the diffusion term F_D with any combination of the term F_A, F_R and that also treats Itô stochastic systems of the form

$$\dot{y} = F(y) = F_D(y) + F_A(y) + F_R(y) + \sum_{j=1}^{m} F_G^j(y)\dot{\xi}_j, \quad y(0) = y_0, \tag{2}$$

where $\xi_j, j = 1, \ldots, m$ are independent one-dimensional Wiener processes. The main idea of the new method is to modify the finishing procedure of the standard ROCK2 method, i.e. the final stages of ROCK2 used to achieve the order two of accuracy. We introduce a partitioned RK method, where the diffusion terms F_D and advection terms F_A are treated explicitly, while the reaction terms F_R are treated implicitly.

Compared to similar existing stabilized methods, the PIROCK method has the following features:

- for problems with stiff reactions, the number of function evaluations of the reaction terms F_R (solved implicitly) is independent of the stage number s used to handle the stiffness of the diffusion terms F_D (in contrast, the number of implicit stages in each step of the IRKC method is equal to s);
- for advection dominated problems, the PIROCK method is more efficient than the RKC or ROCK2 solvers as it has better stability in the imaginary direction and requires a number of evaluations of the advection terms that is independent of the stage number of the method; compared to the PRKC method [12], the PIROCK method has larger stability domains on both the real and the imaginary parts;
- for problems with expensive evaluation of (non-stiff) reaction terms PIROCK is more efficient than RKC [4] or ROCK2 [5] as the number of evaluation of the reaction terms is independent of the stage number of the method; for such problems, it is comparable to the PRKC method [12] but has larger stability along the negative real axis;
- for problems involving white noise, it is more efficient than previously constructed S-ROCK methods [13,14], as PIROCK has a larger mean–square stability domain.

We emphasize that the methods RKC, ROCK2, PRKC are not efficient for problems with severely stiff reactions, while the RKC, IRKC, and ROCK2 methods are not efficient for problems for which the reaction is not stiff but is very costly to evaluate.

In addition, notice that a common assumption for all known explicit stabilized integrators is that the differential operator is (nearly) symmetric and has eigenvalues close to the negative real axis. In the case of a non-symmetric differential operator the eigenvalues of the Jacobian of F_D are typically located in a sector

$$S_\theta = \{-\rho e^{i\tau}; \rho \geqslant 0, -\theta \leqslant \tau \leqslant \theta\} \tag{3}$$

of the left half complex plane, where $\theta \leqslant \pi/2$ is the angle of this sector. If θ is close to zero then the differential operator is nearly symmetric and the standard stabilized integrators like RKC and ROCK2 can be applied (using more damping if needed, to enlarge the stability domain in the imaginary direction). We shall show that the PIROCK method can also be extended to non-symmetric diffusion operators in sectors (3) for large angles up to $\theta = \pi/4$.

The proposed PIROCK algorithm is versatile and efficient (hence the " swiss-knife") in handling problems such as (1) for various regimes with a single code. It is fully adaptive and requires no tuning from the user. Appropriate error estimators take care of the stiff and non-stiff components of the problems as to deliver a variable step size aiming at an integration error of the size of a tolerance given by the user. While efficient stabilized integrators for special regimes of (1) are available, none has existed until now for the various potential regimes of (1). We also emphasize that PIROCK is more than a simple combination of integrators developed in [7,14,15,12], as the coupling of the different regimes requires new ideas to stabilize the various possible combinations of the dynamics in (1).

The rest of the paper is organized as follows. In Section 2 we briefly recall the concept of partitioned RK methods, explicit stabilized RK methods and linear stability analysis for numerical integrators. In Section 3 we derive step by step the PIROCK method. Finally a number of numerical experiments taken from benchmark problems for ROCK2, SROCK, RKC, IRKC, PRKC, presented in Section 4 illustrate the flexibility and the performance of PIROCK.

2. Preliminaries

In this section we present the background concepts needed for the PIROCK integrators, namely a short description of the ROCK2 integrator, linear stability analysis and partitioned Runge–Kutta methods.

2.1. ROCK2 methods

We first describe an efficient explicit stabilized method for ODEs (2) for the problem

$$\dot{y} = F(y), \quad y(0) = y_0, \tag{4}$$

assuming that the Jacobian of $F(y)$ has its eigenvalues close to the real negative axis (with possibly large modulus). We recall that linear stability analysis for stiff ODEs is usually studied on the linear scalar test equation $y' = \lambda y, y(0) = 1$, that can be obtained from linearization and diagonalization (or transformation to Jordan form) of a system of ODEs. The value of λ represents a typical eigenvalue of the Jacobian of the linearized system and a stable mode (i.e. for $\Re\lambda \leqslant 0$) should be damped by the numerical solver for stability. A RK method applied to the linear test problem leads to the recursion

$$y_{n+1} = R(z)y_n, \tag{5}$$

where $z = h\lambda$, and $R(z)$ is a rational function called the stability function of the numerical method (notice that it is a polynomial for an explicit method). This allows to define the stability domain of the numerical integrator as

$$\mathcal{S} := \{z \in \mathbb{C}; |R(z)| \leqslant 1\} \tag{6}$$

and the numerical solution $\{y_n\}$ in (5) is bounded for $n \to \infty$ if and only if $z \in \mathcal{S}$. If $\{z \in \mathbb{C}; \Re z \leqslant 0\} \subset \mathcal{S}$, then the method is called A-stable, and this is a desirable property for stiff problems. If in addition $\lim_{z\to\infty} R(z) = 0$, the method is called L-stable. This latter property is also desirable for stiff problems because it permits a numerical damping of the rapidly decaying eigen modes.

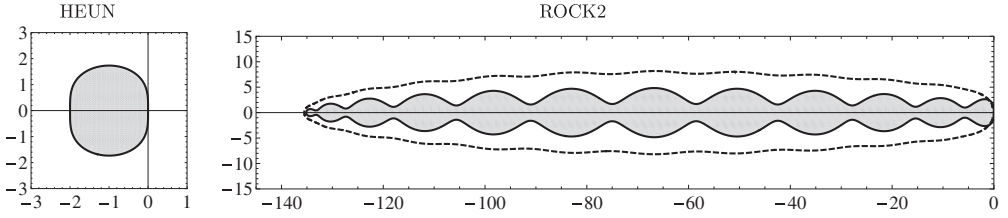

Fig. 1. Complex stability domains (gray regions) of a standard second order explicit method (Heun method, left picture) versus an explicit stabilized method (ROCK2 with damping $r = 0.95$ ($\alpha = 1$) for $s = 13$. Right picture: the dashed line indicate the stability domain boundary of the embedded method used for step size control (see Section 3.3).

Classical explicit methods have a restricted stability domain (6) along the negative real axis as illustrated in Fig. 1 (left picture) for the second order Heun method, where $R(z) = 1 + z + z^2/2$, resulting in a severe step size restriction for stiff problems. Stabilized methods allow to increase the stability domains along the negative real axis in an adaptive way, to accommodate stiff dissipative problems without facing step size restriction. An early first order stabilized method [4] is based on the following recursion

$$\begin{aligned} K_1 &= y_0 + h\frac{\omega_1}{\omega_0}F(y_0),\\ K_j &= 2h\frac{T_{j-1}(\omega_0)}{T_j(\omega_0)}F(K_{j-1}) + 2\omega_0\frac{T_{j-1}(\omega_0)}{T_j(\omega_0)}K_{j-1} - \frac{T_{j-2}(\omega_0)}{T_j(\omega_0)}K_{j-2}, \quad j = 2\dots s,\\ y_1 &= K_s, \end{aligned} \tag{7}$$

where $K_0 = y_0, T_s(\cos x) = \cos(sx)$ are the classical Chebyshev polynomials, $s \geqslant 1$ is the number of stages, $\eta \geqslant 0$ is a damping parameter (discussed below) and $\omega_0 = 1 + \frac{\eta}{s^2}, \omega_1 = \frac{T_s(\omega_0)}{T_s'(\omega_0)}$. Applied to the above linear test problem the method (7) gives $y_1 = R_s(z)y_0$, where $z = \lambda h$ and $R_s(z)$ is given by $R_s(z) = T_s(\omega_0 + \omega_1 z)/T_s(\omega_0)$ and satisfies

$$|R_s(z)| \leqslant 1 \text{ forall } z \in (-d_s, 0),$$

with $d_s \simeq C \cdot s^2$, for s large enough, where C depends on the damping parameter η (for $\eta = 0, C = 2$). Notice that (7) represents a family of numerical methods (indexed by the stage number s) and the stability domain size d_s along the negative real axis grows quadratically with s.

Damping. It has been realized in the early development of the stabilized method that it is desirable to introduce a damping of the higher frequencies and include an ellipse around the negative real axis in the stability domain, i.e., to consider

$$|R_s(z)| \leqslant r < 1 \text{ for all } z \in (-d_s, -\varepsilon), \tag{8}$$

where ε is a small positive number (observe that $R_s(0) = 1$). For instance, for the method (7), we have that $r = T_s(\omega_0)^{-1} < 1$ in (8) is a decreasing function of $\eta > 0$. This reduces the constant C in $d_s \simeq C \cdot s^2$, but the boundary of the stability domains does not intersect with the negative real axis (except at the two endpoints).

Constructing higher order stabilized methods is a non-trivial task and various strategies have been proposed. We mention the RKC method [4] and the DUMKA method [3]. We describe here the ROCK2 method introduced in [5] and generalized to fourth order in [6]. It will be used in what follows. It combines the second order optimal stability domains of [3] with a realization based on a three term recursion formula (similarly as in [4]). The stability function of the ROCK2 method reads

$$R_s(z) = P_{s-2}(z)w_2(z), \tag{9}$$

where P_{s-2} belongs to the family of polynomials $\{P_j\}_{j\geqslant 0}$ (depending on s) orthogonal with respect to the weight function $\frac{w_2(x)^2}{\sqrt{1-x^2}}$. The polynomial w_2, which depends on s, is positive on $\mathbb{R}$ and has degree 2. It is chosen such that R_s satisfies [5]

$$R_s(z) = 1 + z + \frac{z^2}{2} + \mathcal{O}(z^3), \quad z \to 0, \tag{10}$$

together with a large stability interval (8). The recurrence relation of the orthogonal polynomials $\{P_j\}_{j\geqslant 0}$ enables the construction of a RK method $y_0 \mapsto y_1$ of order two for (4) based on the following recursion for $s \geqslant 3$,

$$\begin{aligned} K_1 &= y_0 + \mu_1 hF(y_0),\\ K_j &= \mu_j hF(K_{j-1}) - \nu_j K_{j-1} - \kappa_j K_{j-2}, \quad j = 2\dots s-2,\\ K^*_{s-1} &= K_{s-2} + \sigma hF(K_{s-2}),\\ K^*_s &= K^*_{s-1} + \sigma hF(K^*_{s-1}),\\ y_1 &= K^*_s - \sigma(1-\tau/\sigma^2)\big(hF(K^*_{s-1}) - hF(K_{s-2})\big), \end{aligned} \tag{11}$$

where $K_0 = y_0$. The parameters μ_j, κ_j, ν_j (depending on s) are obtained from the three-term recurrence relation [5, Eq. 24-25] of the orthogonal polynomials $\{P_j\}_{j\geqslant 0}$, while σ, τ (which also depend on s) satisfy $w_2(z) = 1 + 2\sigma z + \tau z^2$ and are chosen such that (10) holds. We notice that the polynomials $P_j(z)$ are the stability functions of the internal stages $K_j, j = 1, \dots, s-2$. We have for $3 \leqslant s \leqslant 200, \sigma \in (0.367, 0.410)$ and $\tau \in (0.2, 0.4)$. The ROCK2 method satisfies (8) with $d_s \simeq 0.81 \cdot s^2$ for a damping $r = 0.95$, where r is defined in (8). We have thus a family of second order methods, whose stability domains increase quadratically with the stage number s (see Fig. 1 where $d_{13} \simeq 135.1 \simeq 0.81 \cdot 13^2$). As shown in [5], due to the aforementioned stability behavior, this method is competitive with implicit solvers for diffusion problems, while remaining explicit.

As the parameters $\mu_j, \nu_j, \kappa_j, \tau_j, \sigma_j$ depend on r and are computed once and imported into the computer code, changing the value of r requires a priori to recompute these parameters. We explain next a procedure that allows to change the damping with the already precomputed parameters included in the ROCK2 code `http://anmc.epfl.ch`. This idea, first used in [16] for weak second order stochastic stabilized methods, is to consider for (4) the following scheme for a fixed scalar parameter α:

$$
\begin{aligned}
&K_1 = y_0 + \alpha\mu_1 hF(y_0),\\
&K_j = \alpha\mu_j hF(K_{j-1}) - \nu_j K_{j-1} - \kappa_j K_{j-2}, \quad j = 2,\dots,s-2,\\
&K^*_{s-1} = K_{s-2} + \sigma_\alpha hF(K_{s-2}),\\
&K^*_s = K^*_{s-1} + \sigma_\alpha hF(K^*_{s-1}),\\
&y_1 = K^*_s - \sigma_\alpha(1-\tau_\alpha/\sigma_\alpha^2)\big(hF(K^*_{s-1}) - hF(K_{s-2})\big),
\end{aligned}
\tag{12}
$$

where $K_0 = y_0$. Notice that for $\alpha = 1$, we recover the original ROCK2 method (11). Applied to the linear test problem this method yields

$$
y_1 = P_{s-2}(\alpha z)(1 + 2\sigma_\alpha z + \tau_\alpha z^2) =: R_{s,\alpha}(z) \tag{13}
$$

and it can be easily verified (see [16, Lemma 3.2]) that the method (12) has second order for the system of ODEs (2) for any α, provided that

$$
\sigma_\alpha = \frac{1-\alpha}{2} + \alpha\sigma, \quad \tau_\alpha = \frac{(\alpha-1)^2}{2} + 2\alpha(1-\alpha)\sigma + \alpha^2\tau. \tag{14}
$$

For the PIROCK method we will need two additional stages associated to the family of orthogonal polynomials $\{P_j\}_{j\geqslant 0}$,

$$
K_j = \alpha\mu_j hF(K_{j-1}) - \nu_j K_{j-1} - \kappa_j K_{j-2}, \quad j = s-1, s. \tag{15}
$$

Applied to the linear test problem we obtain

$$
K_{s-1} = P_{s-1}(\alpha z), \quad K_s = P_s(\alpha z). \tag{16}
$$

These polynomials decay faster to zero than $P_{s-2}(\alpha z)$ for z close to zero because $P'_{s-2}(0) < P'_{s-1}(0) < P'_s(0)$, as illustrated in Fig. 2.

It should be noted that the stability function (13) of the ROCK2 methods oscillates for real $p \leqslant 0$ around 0 (see Fig. 2) while the stability functions of other stabilized methods such as the RKC that reads $R_s(z) = a_s + b_s T_s(\omega_0 + \omega_1 z)$, for appropriate ω_0, ω_1 and $a_s = 1 - b_s T_s(\omega_0), b_s = T''_s(\omega_0)/(T'_s(\omega_0))^2$ (see [4,7]) oscillates around the value $a_s > 0$. In turn, these methods have less favorable damping, and the ellipse that can be included in the stability domain is smaller than the corresponding ellipse for the ROCK2 methods.

Implementation of the ROCK2 method. We emphasize that an efficient implementation relies on both stage and time step adaptivity as summarized in the following algorithm. Given the value y_0, the initial step size h, and the required accuracy *tol* (prescribed by the user),

1. perform an integration step $y_0 \to y_1$;
2. estimate the local error $err := \|y_1 - \hat{y}_1\|$;
3. determine a new step size h_{new} such that $err \simeq tol$ based on a step size control strategy;
4. estimate the spectral radius ρ of the Jacobian of F and choose a stage number such that $h_{new}\cdot\rho \simeq C\cdot s^2_{new}$ (where C depends on α);
5. back to 1.

A few comments are in order. First, $\hat{y}_1$ is the numerical solution obtained from a so-called embedded method that allows to estimate the local error. This numerical solution given by $\hat{y}_1 = K^*_s$ in (11) does not involve any significant computational overhead and is obtained from the function evaluations needed for y_1 [17, II.4]. Second, sophisticated procedures are available to compute h_{new} that also take into account previously computed step sizes (memory step size selection) [1, IV.8]. These procedures have proven successful for ROCK2 methods [5]. Third, a precise estimation of the spectral radius (which would be expensive) is not needed. It is sufficient to consider an upper bound that can be provided by the user or obtained from a power methods, using the function evaluations needed for the internal stages [5]. Hence this procedure comes with a negligible cost.

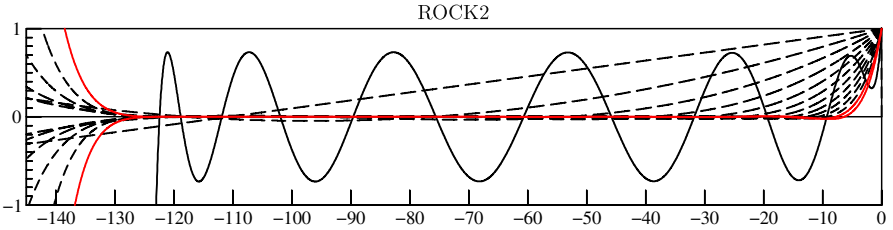

Fig. 2. Stability polynomials for the ROCK2 method with parameters $s = 13, \alpha = 1.2$. The oscillating polynomial is $R_{s,\alpha}(z)$, the dotted lines correspond to the stability polynomials of the internal stages $P_j(\alpha z), j = 1,\dots,11$. The stability functions $P_{s-1}(\alpha z), P_s(\alpha z)$ of the two supplementary stages K_{s-1}, K_s are depicted in solid (red) lines oscillating with a small amplitude. (For interpretation of the references to color in this figure legend, the reader is referred to the web version of this article.)

Applicability and limit of the stabilized methods. Stabilized methods such as the ROCK, RKC or DUMKA have been primarily introduced for the solution of large dissipative systems (i.e., with eigenvalues of the Jacobian close to the negative real axis). They can be applied to systems such as (1) but become inefficient for problems with a large advection and for problems with a very stiff reaction. Increasing the damping (an idea also used for stochastic methods [13,14]) allows to include larger ellipses in the stability domain of the method [7]. But this comes at the cost of reducing the length of the stability domain along the negative real axis and even so, the size in the imaginary direction of the ellipse that can be included in the stability domain is limited (see Section 3.2). Furthermore, another drawback is that the number of function evaluations is proportional to the number of stages. Notice also that optimal stabilized polynomial functions along the imaginary axis have only a linear growth with respect to the stage number [IV.2,1]. Thus, stabilized explicit integrators have no advantage for pure hyperbolic problems.

2.2. Partitioned Runge–Kutta methods

For the time integration of (1), an m-stage partitioned RK method[2] (which maps y_0 to y_1) is given by

$$K_i = y_0 + h\sum_{j=1}^{m} a_{ij}F_D(K_j) + h\sum_{j=1}^{m} \hat{a}_{ij}F_A(K_j) + h\sum_{j=1}^{m} \bar{a}_{ij}F_R(K_j), \quad i = 1,\dots,m, \tag{17}$$

$$y_1 = y_0 + h\sum_{i=1}^{m} b_i F_D(K_i) + h\sum_{i=1}^{m} \hat{b}_i F_A(K_i) + h\sum_{i=1}^{m} \bar{b}_i F_R(K_i). \tag{18}$$

Remark 1. For a non-autonomous problem, we need to evaluate the stages at discrete time $t_0 + c_i h, t_0 + \hat{c}_i h, t_0 + \bar{c}_i h, i = 1,\dots,m$ and we assume as usual that the conditions $c_i = \sum_{j=1}^{m} a_{ij}, \hat{c}_i = \sum_{j=1}^{m} \hat{a}_{ij}, \bar{c}_i = \sum_{j=1}^{m} \bar{a}_{ij}, i = 1,\dots,m$ are satisfied [17].

The method is said to have order p if for sufficiently smooth problems (1), we have the local error bound

$$\|y(t_0 + h) - y_1\| \leqslant Ch^{p+1}. \tag{19}$$

Order conditions for a partitioned RK method (18) are algebraic conditions on the coefficients such that (19) is satisfied for a given p. As we will construct second order methods, we recall the corresponding order conditions, namely

$$\sum_{i=1}^{m} b_i = \sum_{i=1}^{m} \hat{b}_i = \sum_{i=1}^{m} \bar{b}_i = 1, \quad \sum_{i,j=1}^{m} b_i a_{ij} = \sum_{i,j=1}^{m} \hat{b}_i \hat{a}_{ij} = \sum_{i,j=1}^{m} \bar{b}_i \bar{a}_{ij} = \frac{1}{2}, \tag{20}$$

$$\sum_{i,j=1}^{m} b_i \hat{a}_{ij} = \sum_{i,j=1}^{m} b_i \bar{a}_{ij} = \sum_{i,j=1}^{m} \bar{b}_i a_{ij} = \sum_{i,j=1}^{m} \bar{b}_i \hat{a}_{ij} = \sum_{i,j=1}^{m} \hat{b}_i a_{ij} = \sum_{i,j=1}^{m} \hat{b}_i \bar{a}_{ij} = \frac{1}{2}. \tag{21}$$

The conditions (20) ensure that each individual method (for F_D, F_A, F_R) has second order, while conditions (21) ensure that the coupling of the different terms has the right accuracy. It is customary to write the coefficients of a RK method in a so-called Butcher tableau

$$\begin{array}{c|ccc} c_1 & a_{11} & \dots & a_{1m} \\ \vdots & \vdots & & \vdots \\ c_m & a_{m1} & \dots & a_{mm} \\ \hline & b_1 & \dots & b_m \end{array} \tag{22}$$

Applicability and limit of existing stabilized partitioned methods. In the PRKC method [12], a partitioned procedure allows to make the number of evaluations of the advection (or a non-stiff reaction) independent of the stage number. These methods are efficient for diffusion dominated advection-diffusion reaction problems with non-stiff reaction, particularly if the reaction or advection term is costly to evaluate. For dominant advection, the performance of the PRKC method deteriorates (as for the ROCK2 or RKC methods) because of the limited height of the ellipse that can be included in the stability domains of the method. On the other hand the implicit–explicit IRKC method [10] can accommodate stiff reactions (done implicitly) but the number of nonlinear systems to be solved depends on the stage number used to treat the stiffness arising from the diffusion. As for the PRKC method, the performance of the IRKC also deteriorates for problems with dominant advection.

3. The PIROCK method

In this section we derive our new PIROCK method and analyze its stability behavior. We also discuss a posteriori error estimates via embedded RK methods and step size control.

[2] In the literature, integrators of the type 17,18 are sometimes called additive RK methods, while partitioned RK methods refer to integrators for systems of the form $\dot{p} = f(p,q,\dots), \dot{q} = g(p,q,\dots),\dots$Notice however that the order conditions are equivalent [1].

3.1. Derivation of the PIROCK method

We explain step by step the construction of our new methods for the solution of (1).

Step 1: choosing the F_A and F_R methods. We consider the following classical basic methods

F_A–method

0			
$\frac{1}{3}$	$\frac{1}{3}$		
$\frac{2}{3}$		$\frac{2}{3}$	
	$\frac{1}{4}$	0	$\frac{3}{4}$

F_R–method

γ	γ	
$1-\gamma$	$1-2\gamma$	γ
	$\frac{1}{2}$	$\frac{1}{2}$

(23)

where $\gamma = 1 - \sqrt{2}/2$. A 3-stage third order explicit method is taken for the advection (so that a non-empty portion $(-i\sqrt{3}, i\sqrt{3})$ of the imaginary axis is included in the stability domain of the F_A method, see Fig. 3 and a 2-stage second order singly diagonally implicit RK method for the reaction. This latter method is *L*-stable and can be efficiently implemented: due to the diagonal structure of RK coefficients, a single *LU* factorization needs to be done only once per step if using a quasi-Newton method [1].

Step 2: Diffusion step and coupling. In the PIROCK method, we perform the diffusion step first and introduce the advection and reaction steps as a"finishing procedure". This diffusion step needs then to be coupled with the F_A and F_R methods (see the coupling order conditions (21)). We explain the coupling by choosing the (explicit) Heun method for the diffusion steps. This choice is only done here temporarily to simplify the presentation and we emphasize that the Heun method will later be replaced by the ROCK 2 method. For the time being we thus consider

0		
1	1	
	$\frac{1}{2}$	$\frac{1}{2}$

(24)

The partitioned method with the Heun method for the diffusion step and the F_A, F_R methods as finishing procedure together with suitable coupling conditions reads

F_D–method

0								
1	1							
0								
1		1						
0								
0								
$\frac{2}{3}$		$\frac{2}{3}$						
1	1							
	$\frac{1}{2}$	$\frac{1}{2}$	$-\frac{1}{2(1-2\gamma)}$	0	$\frac{1}{2(1-2\gamma)}$	0	0	0

(25)

F_A–method

0								
0								
0								
1		1						
$1-2\gamma$		$1-2\gamma$						
$\frac{1}{3}$		$\frac{1}{3}$						
$\frac{2}{3}$				$\frac{2}{3}$				
0								
	0	0	$\frac{1}{4}$	0	0	0	$\frac{3}{4}$	0

F_R–method

0								
0								
γ		γ						
$1-\gamma$		$1-2\gamma$	γ					
$1-\gamma$		$1-\gamma$						
0								
$\frac{2-\gamma}{3}$		$\frac{2}{3}-\gamma$	$\frac{2\gamma}{3}$					
0								
	0	0	$\frac{1}{2}$	$\frac{1}{2}$	0	0	0	0

(26)

where $\gamma = 1 - \sqrt{2}/2$. Of course this choice of coupling is by no mean unique. We make the above choice of coupling because it has the same cost as each of the 3 non-partitioned RK methods (24), (23), with the exception that two extra evaluations of the diffusion function F_D are needed at each step. The coefficients $\frac{2}{3} - \gamma, \frac{2\gamma}{3}$ in the F_R-method are chosen to make the corresponding internal stage *L*-stable with respect to the reaction F_R.

Step 3: Introducing a perturbation of the initial value for F_A and F_R. The above partitioned method (25,26) takes y_0 as initial value for the advection and the reaction part. The idea of the PIROCK algorithm is to use internal stages of the ROCK2 method for the stabilization of the coupling with the reaction and advection terms. It is thus of interest to start with a suitably perturbed initial value, say $y_0 + \delta h F_D(y_0)$, where δ is a fixed real. The partitioned method is then given by the following F_D-method together with the unchanged F_A and F_R tableau in (26),

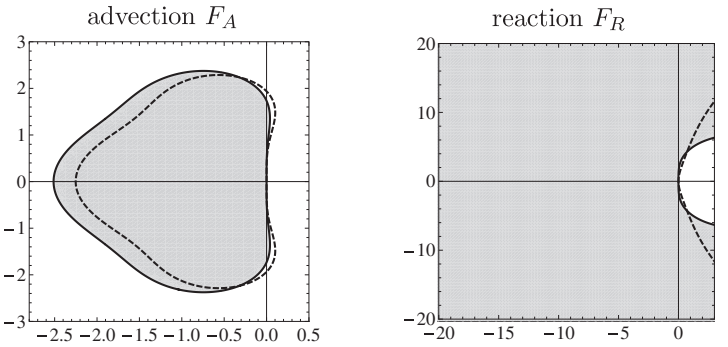

Fig. 3. Complex stability regions for the F_A and the F_R when applied to the linear test problem The dashed lines indicate the boundaries of the error estimator stability domains (see Section 3.3).

F_D–method

$$\begin{array}{c|cc} 0 & & \\ \delta & \delta & \\ \hline \delta & \delta & \\ \delta+\beta & \delta & \beta \\ \delta & \delta & \\ \delta & \delta & \\ \delta+\frac{2}{3}\beta & \delta & \frac{2}{3}\beta \\ 1 & 1 & \end{array} \qquad \begin{array}{c|cccccc} \frac{1}{2} & 0 & -\frac{1}{2(1-2\gamma)} & 0 & \frac{1}{2(1-2\gamma)} & 0 & \frac{1}{2} \\ \hline & & & & & & \end{array} \tag{27}$$

A new parameter β has been introduced to maintain the second order accuracy for the coupling of the diffusion–advection and diffusion–reaction terms with an arbitrary value of δ. It can be again easily verified that the above method has second order (i.e., (20) and (21) hold) for arbitrary δ provided

$$\beta = 1 - 2\delta. \tag{28}$$

Efficient resolution of the nonlinear systems. We notice that for each step of the above method (26,25), we have to solve two nonlinear systems of the type

$$y = c_j + \gamma h F_R(y), \tag{29}$$

where c_j $(j = 1, 2)$ is independent of y. The resolution can be done efficiently because the nonlinear systems for each spatial component are independent. This means that (29) consists of decoupled systems in low dimension $n_{PDEs} \ll n$, where n_{PDEs} is usually given by the number of scalar PDEs in a system of PDEs, and n is the dimension of the system after spatial discretization. It can be performed using a quasi-Newton method $J_R(y^{k+1} - y^k) = -y^k + c_j + \gamma h F_R(y^k)$ where the *LU* decomposition of the matrix

$$J_R = I - \gamma h \frac{\partial F_R}{\partial y}(c_1) \tag{30}$$

has to be computed only once per step size. Notice that in contrast, the IRKC method requires at each time step the resolution of s nonlinear systems of the form (29) where s is the number of stages. In addition, the LU decomposition of the matrix J_R has to be computed s times per step of IRKC because the systems (29) use different values of the coefficient γ in each stage. *Using J_R^{-1} for stabilization.* It has been noticed by Shampine (as presented in [1, IV.8]) that J_R^{-1} can also be used for stabilization purpose (originally used for the error control). In the PIROCK method, J_R^{-1} will also be used to further stabilize the coupling of the diffusion step with the F_A and F_R methods. We emphasize that computing $J_R^{-1} v$, for a given vector v represents *a negligible cost* as the LU factorization of J_R is already available from the computation of the implicit stages (29). Likewise computing a higher order power such as J_R^{-2} comes also with a negligible cost.

Step 4: Stabilizing the partitioned method and definition of the PIROCK method. Although based on good methods for the advection and reaction part of the ODE (1), the method (26,27) is useless because of its poor stability for the diffusion part. The PIROCK method is based upon the following modification of the method (26,27):

- replacement of the Heun method (24) with the ROCK2 method (12) in which we compute the two additional stages K_{s-1}, K_s in (15);
- choice of the starting value for the advection and reaction terms at K_s (or K_{s-1});
- use of $J_R^{-\ell} = \left(I - \gamma h \frac{\partial F_R}{\partial y}\right)^{-\ell}, \ell = 1, 2$ to stabilize the couplings F_D–F_R, F_A–F_R.

PIROCK integrator. The partitioned integrator for (1) is defined by the following algorithm for $s \geqslant 3$:

$$
\begin{aligned}
&\texttt{Diffusion stabilization procedure}\\
&K_1 = y_0 + \alpha\mu_1 hF_D(y_0), \quad K_0 = y_0,\\
&K_j = \alpha\mu_j hF_D(K_{j-1}) - \nu_j K_{j-1} - \kappa_j K_{j-2}, \quad j = 2,\dots,s-2+\ell \quad (\ell = 1 \text{ or } 2)\\
&\texttt{Finishing procedure for diffusion}\\
&K^*_{s-1} = K_{s-2} + \sigma_\alpha hF_D(K_{s-2}),\\
&K^*_s = K^*_{s-1} + \sigma_\alpha hF_D(K^*_{s-1}),\\
&\texttt{Starting value for advection} - \texttt{reaction}\\
&K = K_{s-2+\ell},\\
&\texttt{Finishing procedure for advection} - \texttt{reaction and coupling}\\
&K_{s+1} = K + \gamma hF_R(K_{s+1}),\\
&K_{s+2} = K + \beta hF_D(K_{s+1}) + hF_A(K_{s+1}) + (1-2\gamma)hF_R(K_{s+1}) + \gamma hF_R(K_{s+2}),\\
&K_{s+3} = K + (1-2\gamma)hF_A(K_{s+1}) + (1-\gamma)hF_R(K_{s+1}),\\
&K_{s+4} = K + \frac{1}{3}hF_A(K_{s+1}),\\
&K_{s+5} = K + \frac{2\beta}{3}hF_D(K_{s+1}) + \frac{2}{3}hJ_R^{-1}F_A(K_{s+4}) + \left(\frac{2}{3}-\gamma\right)hF_R(K_{s+1}) + \frac{2\gamma}{3}hF_R(K_{s+2})\\
&\texttt{Computation of the integration step } y_0 \mapsto y_1\\
&y_1 = K^*_s - \sigma_\alpha(1-\tau_\alpha/\sigma_\alpha^2)(hF_D(K^*_{s-1}) - hF_D(K_{s-2})) + \frac{1}{4}hF_A(K_{s+1}) + \frac{3}{4}hF_A(K_{s+5}) + \frac{1}{2}hF_R(K_{s+1}) + \frac{1}{2}hF_R(K_{s+2})\\
&\qquad + \frac{J_R^{-\ell}}{2-4\gamma}(hF_D(K_{s+3}) - hF_D(K_{s+1})),
\end{aligned}
\tag{31}
$$

where μ_j, ν_j, κ_j are the same coefficients as for the standard ROCK2 method (12), the coefficients $\sigma_\alpha, \tau_\alpha$ are defined in (13), $\gamma = 1 - \sqrt{2}/2$, $\beta = 1 - 2\alpha P'_{s-2+\ell}(0)$ and $J_R = I - \gamma h\frac{\partial F_R}{\partial y}(K_s)$.

We notice that the starting value for the advection and the reaction term requires the stage K of the ROCK2 method. We shall consider two choices of parameters $\alpha \geqslant 1$ (see (12)) and with corresponding values $\ell = 1$ or 2 in (31). The first choice is

$$\alpha = 1, \quad \ell = 2, \tag{32}$$

which permits to recover the standard ROCK2 method in the absence of advection and reaction terms ($F_A = F_R = 0$), with a (close to optimal) stability domain along the negative real axis of size $d_s \simeq 0.81 \cdot s^2$. The second choice that we shall consider is

$$\alpha = 1/(2P'_{s-1}(0)), \quad \ell = 1. \tag{33}$$

This is a regime with larger damping ($\alpha > 1$) than in the standard ROCK2 method and allows to includes a larger ellipse in the stability domain of the method for the coupling F_D–F_A. It is thus suited for advection dominated problems. Observe also that for this choice of damping, $\beta = 0$.

Remark 2. The choice of values $\ell = 1$ or 2, used for the definition of the internal stage K in (31), is made to provide a better damping in the stability domains close to the origin. Since $P'_{s-2+\ell}(0) > P'_{s-2}(0)$, the stability polynomial $P_{s-2+\ell}$ associated to K decays faster close to the origin than the one associated to K_{s-2} and involved in the ROCK2 method (see Fig. 2). This permits to avoid a gap in the stability domains close to the origin for the F_D–F_A and F_D–F_R couplings. Also, the choice of the negative power $J_R^{-\ell}$ in (31) is made to avoid a gap in the stability domains involving the F_D–F_R coupling, while the term J_R^{-1} in K_{s+5} is used to stabilize the F_A–F_R coupling.

Complexity. Compared to the standard ROCK2 method (12), the PIROCK method requires at each time step $2+\ell$ additional evaluations of F_D (with $\ell = 1$ or 2), 3 evaluations of F_A, and 2 resolutions of a nonlinear system of the form (29) that are usually computationally cheap (see (30)). In contrast, the IRKC method requires the resolution of s nonlinear system of the form (29) (with different values of γ at each internal stage) where s is the number of stages of the IRKC method.

Accuracy. We next verify that the PIROCK method is indeed second order accurate.

Theorem 3.2. *The method (31) has second order of accuracy for (1).*

Proof. We notice that (31) is a perturbation of the second order method (26,27), now involving J_R^{-2}, with the second order Heun method replaced by the second order ROCK2 method (12) and with K_2 replaced with K. A simple expansion using (16) shows that

$$K = y_0 + \alpha hP'_{s-2+\ell}(0)F_D(y_0) + \mathcal{O}(h^2)$$

and thus, in view of (28) where $\delta = \alpha P'_{s-2+\ell}(0)$, we need to define $\beta = 1 - 2\alpha P'_{s-2+\ell}(0)$. Finally, involving the matrix J_R^{-1} only introduces a perturbation of size $\mathcal{O}(h^3)$ in y_1 because J_R^{-1} is a $\mathcal{O}(h)$-perturbation of the identity and the proof is complete. □

Remark 3.3. Theorem 3.2 states the second order of accuracy of the PIROCK method for systems of ODEs. Notice however that the analysis of the dependency of the error constant on the stiffness of the problem is out of the scope of the paper. We mention that the second order error constant of the F_R-method itself, defined in (23), can be shown to be independent of the stiffness using the theory of B-convergence (see [18, p. 31]). The error constant of the RKC method is shown to be independent of the stiffness for a class of linear problems in [19]. This is extended to classes of explicit stabilized methods (including ROCK2) in [20] in the context of multiscale homogenization problems.

Extension to non-symmetric diffusion operators. We explain now a simple modification of the PIROCK algorithm to treat the case of a non-symmetric diffusion operator. Assume that the diffusion operator can be decomposed as

$$F_D(y) = F_{D_S}(y) + F_{D_A}(y), \tag{34}$$

where the eigenvalues of the Jacobians of F_{D_S} and F_{D_A} are located respectively on the negative real axis and the imaginary axis. For instance, in the case of the differential operator $\mathrm{div}(a\nabla\cdot)$, where a is a non-symmetric $N \times N$ tensor, the corresponding decomposition reads $\mathrm{div}(\frac{a+a^T}{2}\nabla\cdot) + \mathrm{div}\left(\frac{a-a^T}{2}\nabla\cdot\right)$. Then, we introduce the following modifications in the definition of the PIROCK algorithm (31) for the damping (33). First, we replace F_D by F_{D_S} in all stages. Next, we replace F_A by $F_A + F_{D_A}$ in the formulas for K_{s+2}, K_{s+3}, and y_1. Finally, in the stage K_{s+5}, we substitute $F_A(K_{s+4})$ by $F_A(K_{s+4}) + F_{D_A}(K_{s+1})$. Notice that this modification remains explicit. The stability analysis of this modification for non-symmetric tensors is addressed in the next Section 3.2.

Extension to stochastic problems. The PIROCK method can also be used for stiff mean–square stable Itô stochastic SDEs of the form (2). The stochastic version of PIROCK, a map from $y_0 \mapsto y_1^*$, is obtained by modifying the last line of the PIROCK integrator (31) as follows

$$y_1^* = y_1 + \sum_{j=1}^{m} F_G^j(K_{s+1}^*)\Delta W_j, \tag{35}$$

where y_1 is defined in (31), and using the supporting value

$$K_{s+1}^* = J_R^{-1}(K_{s+1} + \beta h F_D(K_{s+1})),$$

where $\Delta W_i \sim \mathcal{N}(0,h)$ are independent Wiener increments, and J_R is the block diagonal matrix in (30) whose LU decomposition has been already computed. The term $\beta h F_D(K_{s+1})$, already computed before, is used to avoid a small gap in the mean-square stability domain close to the origin in the F_D–F_G coupling. The multiplication with J_R^{-1} is used to stabilize the F_R–F_G coupling and make it mean–square A-stable with respect to this coupling (see below). It is easily seen that the integrator (35) has weak order 1 and strong order $1/2$ for general Itô stochastic SDEs of the form (2). We refer to [14,13] for accuracy concepts and more details on stabilized stochastic methods. Notice that an explicit stabilized method of weak order 2 with extended mean-square stability domains was recently constructed in [16].

3.2. Stability analysis

We analyze here the stability of the various couplings in the method (31). To analyse the coupling of the diffusion term F_D respectively with F_A, F_R, F_G, we shall consider scalar linear test problems, where $F_D(y) = \lambda y$ is linear and $\lambda \in \mathbb{R}^-$ corresponds to the eigenvalue of a symmetric diffusion operator, and $F_A(y) = i\mu y$ with $\mu \in \mathbb{R}, F_R(y) = \rho y$ with $\rho < 0, F_G = \sigma y$ with $\sigma \in \mathbb{R}$. We emphasize that such test problems only give insight on the stability of the PIROCK method, because the operators involved in problem (1) cannot in general be put simultaneously into diagonal form (even in the case where they are linear).

Diffusion–advection coupling. For the F_D–F_A coupling, we consider the test problem

$$\dot{y}(t) = \lambda y(t) + i\mu y(t),$$

where $\lambda \in \mathbb{R}_-, \mu \in \mathbb{R}$. This test equation is relevant for advection–diffusion equations

$$\partial_t u(x,t) + v\partial_x u(x,t) = \partial_{xx} u(x,t), \quad x \in (0,1), t > 0, \tag{36}$$

as the linear systems of ODEs arising from the (Fourier) spatial discretization on a uniform grid of size Δx has eigenvalues that belong to the ellipse

$$\left(\frac{2p}{d} + 1\right)^2 + \left(\frac{q}{a}\right)^2 = 1 \tag{37}$$

with half-height $a = v\Delta x^{-1}$, and width $d = 4\Delta x^{-2}$. To study the stability of a given advection–diffusion integrator, a natural criteria is to search for the largest ellipse included in the stability domain of the method for the scalar test problem

$\dot{y} = \lambda y + i\mu y$, where (p,q) belongs to the ellipse (37), with $p = h\lambda, q = h\mu$. Precisely, we search for the ellipse first with the largest width d, and then with the largest half-height a.

The PIROCK method (31) then yields $y_{n+1} = R(p,q)y_n$, where $p = h\lambda, q = h\mu$,

$$R(p,q) = R_{s,\alpha}(p) + P_{s-2+\ell}(\alpha p)\left(-\frac{q^2}{2} + i\left(q - \frac{q^3}{6} + \left(\beta + \frac{1}{2}\right)pq\right)\right) \tag{38}$$

and $R_{s,\alpha}$ is the stability function (13) of the ROCK2 method. We plot in Fig. 4 the corresponding stability domains in the (p,q)-plane, for $s = 13$ and the two choices of damping (32), (33). We also plot the largest stability ellipses (37) included in the stability domains. In Fig. 5, we plot the ellipse parameters a_s, d_s as functions of s for the choices (32) (solid lines) and (33) (dashed lines). We observe that these ellipse parameters as functions of s grow quadratically for the width d_s and linearly for the half-height a_s as

$$d_s \simeq 0.81 \cdot s^2, \quad a_s \simeq 0.07696 \cdot s + 1.878, \quad \text{for the damping (32)}, \tag{39}$$

$$d_s \simeq 0.43 \cdot s^2, \quad a_s \simeq 0.5321 \cdot s + 0.4996, \quad \text{for the damping (33)}. \tag{40}$$

Notice that in [7], the RKC method is considered with a large value $\eta = 10$ of the damping parameter. However, it reduces down to $d_s \simeq 0.34 \cdot s^2$ the length of the stability domain along the negative real axis, and only a growth of size $\mathcal{O}(\sqrt{s})$ is obtained for the ellipse half-height a_s. In contrast, in the PRKC approach [12], the coefficients of the PRKC method are chosen such that the stability domain of the diffusion–advection coupling includes in the (p,q)-plan a rectangle $[-d_s, 0] \times [-b, b]$ of half-height $b = 1.7273$ (close to $\sqrt{3}$), independently of the number of stages s, where $d_s \simeq 0.65 \cdot s^2$ and while keeping the standard damping $\eta = 2/13$ of the standard RKC method. The stability constraint for advection of the PRKC method then reads $h \leqslant b/\rho_A$.

Remark 3.4. The linear growths (39), (40) of the ellipse half-height a_s is a feature of PIROCK that takes advantage of the diffusion terms to stabilize the possibly large advection terms. Indeed, consider in particular the damping (33). Substituting $h\rho_D = 0.43 \cdot s^2$ into $h\rho_A \leqslant \max(0.53 \cdot s, \sqrt{3})$ yields the stability sufficient condition

$$h\rho_A \leqslant \max\left(\frac{0.53^2}{0.43}\rho_D/\rho_A, \sqrt{3}\right).$$

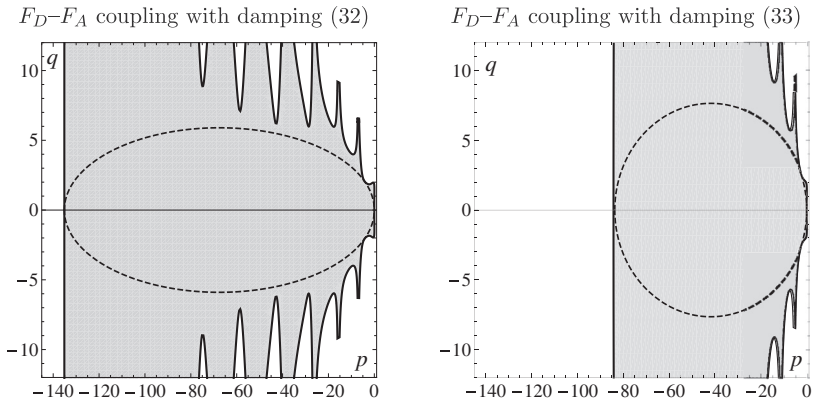

Fig. 4. Diffusion–advection (F_D–F_A) coupling in PIROCK with $s = 13$. Stability domain (dark gray) in the pq–axis. The dotted lines indicate the largest inscribed ellipses. Left picture: damping (32). Right picture: damping (33) where $\alpha \simeq 1.363$.

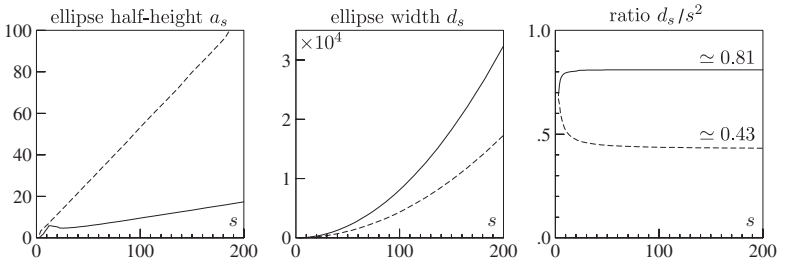

Fig. 5. Diffusion–advection (F_D–F_A) coupling in PIROCK. Half-height and width of the largest ellipse inscribed in the stability domain as a function of the stage parameter s. Solid lines: damping (32). Dashed lines: damping (33).

Considering again the advection–diffusion test problem (36) on a uniform grid of size Δx, using $\rho_A = v\Delta x^{-1}$ and $\rho_D = 4\Delta x^{-2}$, we have that the PIROCK method is stable if $hv \leqslant \max(2.61 \cdot v^{-1}, 1.73 \cdot \Delta x)$ and this stability constraint on the stepsize h is independent of the spatial grid size small enough ($\Delta x \leqslant v^{-1}$), in contrast to the other stabilized explicit integrators RKC, PRKC and ROCK2.

Diffusion–reaction coupling. For the F_D–F_R coupling, we consider the test problem

$$y'(t) = \lambda y(t) + \rho y(t),$$

where $\lambda, \rho \leqslant 0$. Applied to this test problem, the PIROCK method yields the relation $y_{n+1} = R(p,r)y_n$ where $p = h\lambda, r = h\rho$, and

$$R(p,r) = R_{s,\alpha}(p) + P_{s-2+\ell}(\alpha p)\left(\frac{r-\gamma^2 r^2}{(1-\gamma r)^2} + \frac{\beta r p}{2(1-\gamma r)^2} + \frac{pr}{2(1-\gamma r)^{1+\ell}}\right).$$

It can be checked that the stability domain in the (p,r) plane contains the subdomain $(-d_s, 0) \times \mathbb{R}_-$ for both choices of damping (32), (33) (see Fig. 6 for $s = 13$). This means that the PIROCK method is unconditionally stable with respect to $\rho \leqslant 0$. Notice that the stability domain also includes points where $r > 0$ is large enough, this due to the L-stability of the F_R-method.
Stability for a non-symmetric operator. To study the coupling F_{D_S}–F_{D_A} in the decomposition (34), we consider the test problem

$$\dot{y}(t) = \lambda y(t) + i\mu y(t),$$

where $\lambda \in \mathbb{R}_-, \mu \in \mathbb{R}$. The values $\lambda, i\mu$ represent real and imaginary eigenvalues of the Jacobian of F_{D_S}, F_{D_A}, respectively. Applying the modified PIROCK method to the above test equation yields, for $p = h\lambda, q = h\mu$, the stability function

$$R(p,q) = R_{s,\alpha}(p) + P_{s-1}(\alpha p)\left(-\frac{q^2}{2} + i\left(q + \frac{1}{2}pq\right)\right),$$

which is identical to (38) with damping (33), with the exception that the q^3 term no longer appears (thanks to an appropriate modification made in the stage K_{s+5}). We have computed numerically for $3 \leqslant s \leqslant 200$ the largest sector inscribed in the stability domain, given by the angle (see left picture of Fig. 7)

$$\theta_s := \sup\{\theta;\ S_\theta \cap A_s \subset \mathcal{S}\},$$

where $\mathcal{S} = \{p + iq \in \mathbb{C}; |R(p,q)| \leqslant 1\}, A_s = \{p + iq \in \mathbb{C}; -d_s \leqslant p \leqslant 0\}$ and S_θ is the sector defined in (3). We observe that $\theta_s \geqslant \pi/4$ for all $s \geqslant 10$. The corresponding stability domain is plotted in Fig. 7 (right picture) for $s = 13$, where $\theta_{13} \simeq 0.26\pi$.
Stochastic stability. For SDEs such as (2), a widely used concept of stability is the mean–square stability considering the scalar test equation [21–24]

$$\dot{y} = \lambda y + \sigma y\dot{\xi}, \quad y(0) = 1, \tag{41}$$

with fixed complex scalar parameters λ, σ. The exact solution of (41) is said mean–square stable if and only if $\lim_{t\to\infty} \mathbb{E}\left(|y(t)|^2\right) = 0$ and for the problem (41) it can be characterized as the set

$$\mathcal{S}^{MS} = \left\{(\lambda,\sigma) \in \mathbb{C}^2; \Re(\lambda) + \frac{1}{2}|\sigma|^2 < 0\right\}. \tag{42}$$

Applied to the SDE (41), a numerical integrator yields the difference equation [22]

$$y_{n+1} = R(p,q,\xi_n)y_n, \tag{43}$$

where $p = \lambda h, q = \sigma\sqrt{h}, \xi_n \sim \mathcal{N}(0,1)$ are independent random variables, and the mean-square stability domain of a numerical method can be characterized as

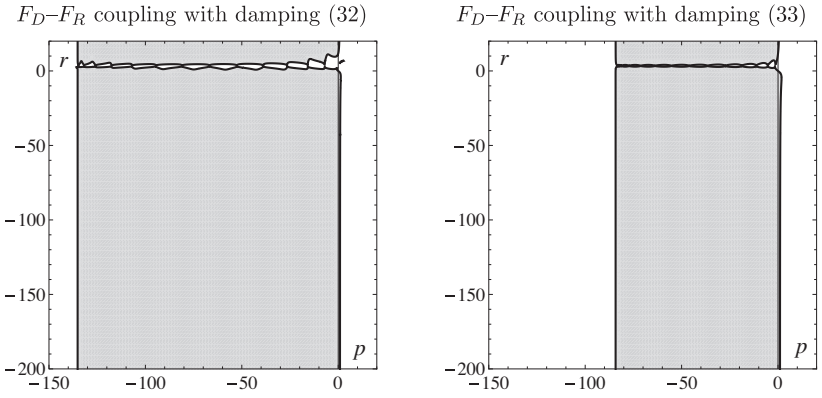

Fig. 6. Diffusion–reaction (F_D–F_R) coupling with $s = 13$. Stability domain in the pr–axis. Left picture: damping (32). Right picture: damping (33).

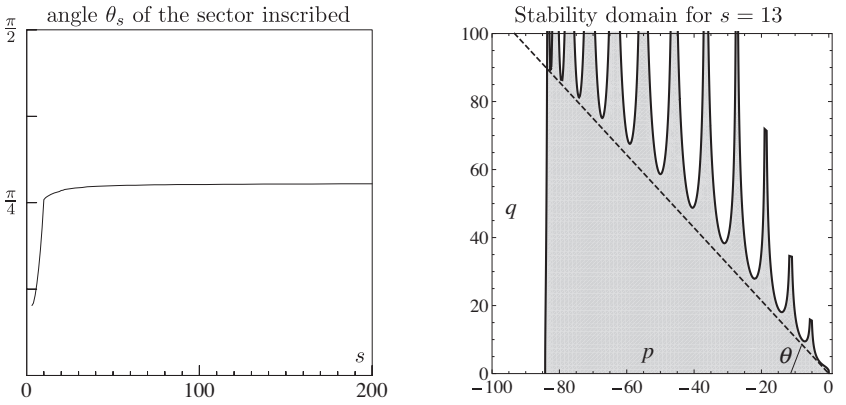

Fig. 7. Case of a non-symmetric differential operator with damping (33) (F_{D_5}–F_{D_A} coupling (34)). Left picture: angle θ_s of the inscribed sector as a function of $\sim s$. Right picture: stability domain in the pq–axis for $s = 13$.

$$\lim_{n\to\infty} \mathbb{E}(|y_n|^2) = 0 \Longleftrightarrow \mathcal{S}^{MS}_{num} := \Big\{(p,q) \in \mathbb{C}^2; \mathbb{E}(|R(p,q,\xi)|^2) < 1\Big\}. \tag{44}$$

If we restrict $(p,q) \in \mathbb{R}^2$ then we consider the portion of the true mean–square stability domain (42), namely

$$\mathcal{S}^{MS}_{x} = \left\{(p,q) \in (-x,0)\times\mathbb{R};\ p + \frac{1}{2}|q|^2 < 0\right\} \tag{45}$$

and define for a given method

$$\ell = \sup\{x > 0;\ \mathcal{S}^{MS}_{x} \subset \mathcal{S}^{MS}_{num}\}, \quad d = \sup\{x > 0;\ (-x,0)\times\{0\} \subset \mathcal{S}^{MS}_{num}\}, \tag{46}$$

where d is the size of the stability domain along the deterministic p-axis (observe that $d \geqslant \ell$). For the diffusion-noise coupling F_D–F_G, the PIROCK method applied to the scalar test problem (41) yields for the mean–square stability function

$$\mathbb{E}(|R(p,q,\xi)|^2) = |R_{s,\alpha}(p)|^2 + |P_{s-2+\ell}(\alpha p)|^2|1+\beta p|^2|q|^2. \tag{47}$$

For $s = 13$, this yields $\ell_{13} \simeq d_{13} \simeq 135.15$, as illustrated in Fig. 8 (left picture) where it can be observed that the portion $\mathcal{S}^{MS}_{\ell_{13}}$ below the dotted line is included in the stability domain. We have checked numerically that the mean-square stability domain $\mathcal{S}^{MS}_{num}$ in (44) contains a portion (45) of the true mean-square stability region of size

$$\ell_s \simeq d_s \simeq 0.81\cdot s^2 \text{using (32)}, \quad \ell_s \simeq d_s \simeq 0.43\cdot s^2 \text{using (33)},$$

as illustrated in Fig. 9. Notice that the S-ROCK method [13], with weak order one and strong order $1/2$, and based on damped first order Chebyshev methods (7), has a shorter mean–square stability domain of size $\ell_s \simeq 0.33\cdot s^2$.

Considering the linear test problem (41) for the reaction-noise coupling F_R–F_G, we obtain the mean–square stability function

$$\mathbb{E}(|R(r,q,\xi)|^2) = \frac{|1+(1-2\gamma)r|^2}{|1-\gamma r|^4} + \frac{|q|^2}{|1-\gamma r|^4}. \tag{48}$$

The corresponding mean–square stability domain $\mathcal{S}^{MS}_{num}$ in (44) can be shown (adapting the proof of Theorem 3.2 [15]) to contain as a subset the exact mean–square stability domain (42), as illustrated in Fig. 8 (right picture). We say that the reaction-noise coupling F_R–F_G is mean–square A-stable.

3.3. Variable step size control

We discuss here variable step size control related to the application of PIROCK to the ODE (1). Adaptive step size for stochastic problems is still to be developed for the PIROCK method and will not be discussed here. To obtain an a posteriori error depending on the computed solution, we use the idea of embedded methods [17]. Considering (18), the idea is to define another set of coefficients $b_i, \hat{b}_i, \bar{b}_i$ say $b_{e,i}, \hat{b}_{e,i}, \bar{b}_{e,i}$ such that the second order non-partitioned order conditions (20) are not fulfilled, but only the first order conditions (except for the advection method where we consider a second order embedded method). We then consider three embedded methods $y_{e,D}, y_{e,A}, y_{e,R}$ where $b_i, \hat{b}_i, \bar{b}_i$ are changed respectively to $b_{e,i}, \hat{b}_{e,i}, \bar{b}_{e,i}$. We obtain for the error estimators $err_D = y_1 - y_{e,D}, err_A = y_1 - y_{e,A}, err_R = y_1 - y_{e,R}$ the values

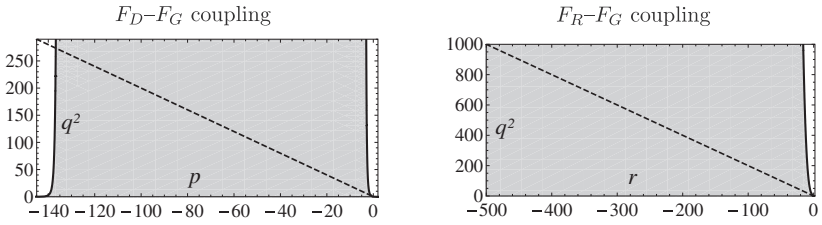

Fig. 8. Mean–square stability domains (gray regions) (44). Left picture: diffusion-noise coupling (stability function (47) with (32) and $s = 13$). Right picture: reaction-noise coupling which is mean–square A-stable (stability function (48)).

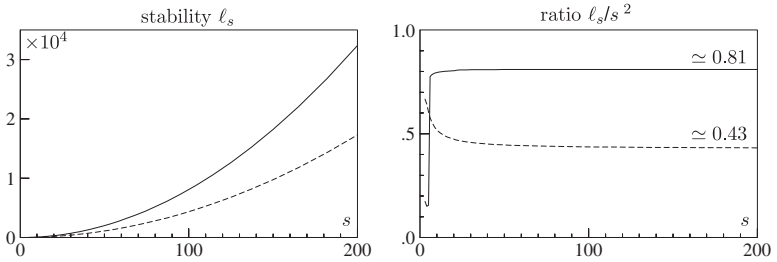

Fig. 9. Diffusion-noise (F_D–F_G) coupling in PIROCK. Length of the portion of the mean–square stability domain. Solid lines: damping (32). Dashed lines: damping (33).

$$
\begin{aligned}
err_D &= \sigma_\alpha(1-\tau_\alpha/\sigma_\alpha^2)(hF_D(K^*_{s-1}) - hF_D(K_{s-2}))\\
err_A &= -\frac{3}{20}hF_A(K_{s+1}) + \frac{3}{10}F_A(K_{s+4}) - \frac{3}{20}F_A(K_{s+5})\\
err_R &= J_R^{-1}\left(\frac{h}{6}F_R(K_{s+1}) - \frac{h}{6}F_R(K_{s+2})\right).
\end{aligned}
\tag{49}
$$

The step size adjustments for adaptive integration are based on the standard strategy (50). Since the order is $p = 2$ for the F_D and F_R methods and $p = 3$ for the F_A method, the step size is selected using

$$
h_{new} = \zeta h(tol/err)^{1/p}, \tag{50}
$$

where $\zeta \in (0.1, 0.8)$ is a safety factor and $p = 2$ is the order of ROCK2 and using the error estimator

$$
err = \max\left(\|err_D\|, \|err_A\|^{2/3}, \|err_R\|\right).
$$

Given the step size h (the initial step size or the adapted step size from (50)), the following selection procedure of PIROCK parameters is implemented in the code, based on the sizes d_s, a_s of the largest ellipses (39) and (40) inscribed in the stability domain of the F_D–F_A coupling:

1. Consider the parameters (32). Select the stage number s such that $d_s \simeq h\rho_D$ (with $d_s \simeq 0.81 \cdot s^2$), where ρ_D is an estimate of the spectral radius of the Jacobian $\partial F_D/\partial y$.
2. If $F_A \neq 0$ and $h\rho_A > a_s$ where ρ_A is an estimate of the spectral radius of $\partial F_A/\partial y$, then consider the damping (33) and select s such that $d_s \simeq h\rho_D$ ($d_s \simeq 0.43 \cdot s^2$).

The choice of estimators (49) is motivated as follows. For the F_D-method we use the embedded method K^*_s in (31) that is identical to the one of the standard ROCK2 method. For the estimator of the F_A-method, we ask that the embedded method has the stability polynomial $1 + z + z^2/2 + z^3/5$. It has order 2 with a similar stability domain as the F_A method (see Fig. 3). For the estimator of the F_R-method, we impose that the embedded method has order one and is A-stable. Since the embedded method is not L-stable, we use Shampine's idea [1, IV.8] and damp it by applying J_R^{-1}, where the LU decomposition of the matrix J_R in (30) (recall that this decomposition is already available, see (30)).

4. Numerical experiments and comparison with other explicit stabilized integrators

We compare our PIROCK integrator with the known time integrators that make an explicit stabilized treatment of the diffusion: RKC, IRKC, PRKC, ROCK2. All these integrators are implemented in FORTRAN and run on the same machine for CPU time comparisons. Unless specified, we use default parameters for all integrators.

4.1. The 2D Brusselator problem with a highly stiff reaction

We consider a modification of the Brusselator problem [1] in 2D with a stiff reaction,

$$\begin{aligned}\frac{\partial u}{\partial t} &= v\Delta u + A + u^2 v - (B+1)u,\\ \frac{\partial v}{\partial t} &= v\Delta v + Bu - u^2 v,\end{aligned} \tag{51}$$

with $x \in (0,1)^2, t \in (0,2), A = 1.3, B = 2\cdot 10^7$, with periodic boundary conditions $u(x_1+1,x_2,t) = u(x_1,x_2,t) = u(x_1,x_2+1,t)$ and the initial condition

$$u(x,0) = 22x_2(1-x_2)^{3/2}, \quad v(x,0) = 27x_1(1-x_1)^{3/2}. \tag{52}$$

For the diffusion, we consider the parameter $v = 10^{-1}$. We discretize u, v in space with two $n \times n$ uniform meshes, where $n = 200$. Here, the vector field F_D corresponds to the discretized Laplacians and the vector field F_R consists of n^2 decoupled reaction ODEs in dimension $n_{PDEs} = 2$. In Fig. 10 and Table 1, we compare the integrators PIROCK and IRKC for the tolerances $tol = 10^{-r}, r = 1,\dots,5$. We take the initial step size $h = 10^{-3}$ for PIROCK, while the step size is automatically selected for IRKC. Notice that the standard integrators RKC,ROCK2 and PRKC cannot be reasonably used because the reaction is too stiff ($B \gg 1$). Indeed, the spectral radius of the Jacobians are for the diffusion $\rho_D = 8n^2 = 3.2\cdot 10^5$, and for the reaction $\rho_R \simeq 10^7$. We point out that large reaction terms, as chosen in the above example, arise in practical applications when very stiff reactions are modeled (see for example [9]).

We observe that the number of evaluations of the diffusion function F_D (column "F_D evals") is reduced by two orders of magnitude for IRKC and PIROCK compared to the standard RKC method. In addition, the PIROCK method compared to IRKC has a considerably reduced number of evaluations of the reaction function F_R and its Jacobian (column "F_R Jac. evals"), by one to two orders of magnitude. This is because the PIROCK method has only two implicit internal stages per step, whereas the IRKC method has all its s internal stages implicit. To check the accuracy of the integrators, we computed independently two reference solutions with tolerance $tol = 10^{-7}$ using PIROCK (95 s of CPU time) and IRKC (1662 s of CPU time), and we checked that the observed errors are identical for both reference solutions.

4.2. A radiation–diffusion problem with a highly stiff reaction

We consider the combustion problem taken from [25], with spatial discretization taken from [2, Chap. 5] and considered for numerical illustrations in [10, Section 4]. This 2D model used in laser fusion applications describes the radiation energy E and the material temperature T, defined on the unit square domain $(0,1)^2$, given by two non-linear diffusion equations with a highly stiff reaction, for $t > 0$,

$$\frac{\partial E}{\partial t} = \nabla\cdot(D_1\nabla E) + \sigma(T^4 - E), \quad \frac{\partial T}{\partial t} = \nabla\cdot(D_2\nabla T) - \sigma(T^4 - E), \tag{53}$$

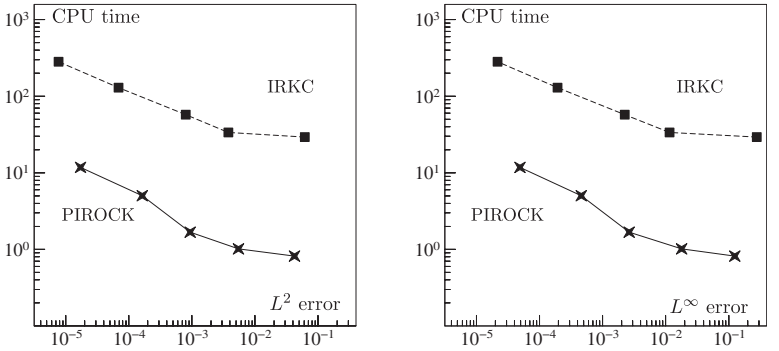

Fig. 10. Comparison of IRKC and PIROCK for the 2D Brusselator problem with a stiff reaction (51). CPU time (seconds) versus L^2 and L^∞ errors for the tolerances $tol = 10^{-r}, r = 1\dots 5$.

Table 1
Comparison of IRKC and PIROCK for the 2D Brusselator problem with a stiff reaction (51).

Method	*tol*	F_D evals	F_R evals	F_R Jac. evals	Steps	s_{max}	L^2 errors	L^∞ errors	CPU times (s)
IRKC	10^{-1}	1045	2134	1044	27(8)	206	$6.2\cdot10^{-2}$	$2.8\cdot10^{-1}$	29.3
PIROCK	10^{-1}	749	55	10	10(0)	182	$4.2\cdot10^{-2}$	$1.3\cdot10^{-1}$	0.8
IRKC	10^{-2}	1175	2443	1174	56(6)	171	$3.8\cdot10^{-3}$	$1.2\cdot10^{-2}$	33.6
PIROCK	10^{-2}	912	75	14	14(0)	150	$5.4\cdot10^{-3}$	$1.8\cdot10^{-2}$	1.0
IRKC	10^{-3}	1952	4295	1951	152(5)	152	$8.0\cdot10^{-4}$	$2.2\cdot10^{-3}$	57.5
PIROCK	10^{-3}	1400	160	31	34(3)	137	$9.3\cdot10^{-4}$	$2.6\cdot10^{-3}$	1.7
IRKC	10^{-4}	3865	10402	3864	462(4)	106	$6.6\cdot10^{-5}$	$1.9\cdot10^{-4}$	129.4
PIROCK	10^{-4}	2845	913	159	161(6)	114	$1.6\cdot10^{-4}$	$4.5\cdot10^{-4}$	5.0
IRKC	10^{-5}	8477	23804	8476	1450(4)	71	$7.5\cdot10^{-6}$	$2.1\cdot10^{-5}$	282.4
PIROCK	10^{-5}	5889	2363	456	458(6)	74	$1.7\cdot10^{-5}$	$4.9\cdot10^{-5}$	11.8

where $\sigma = Z^2/T^3, D_1 = 1/(3\sigma + |\nabla E|/E)$, and $D_2 = kT^{5/2}$ with $k = 0.005$. Here, $Z = Z(x)$ represents the atomic mass number which has the spatial inhomogeneity $Z(x) = Z_0 = 10$ if $\max_j|x_j - 1/2| \leqslant 1/6$, and $Z(x) = 0$ else. For the boundary conditions, we consider homogeneous Neumann boundary conditions for T at all boundaries and for E on the top and bottom boundaries $x_2 = 0, 1$. For the left and right boundaries we consider the nonlinear conditions $\frac{1}{4}E - \frac{1}{6\sigma}\frac{\partial E}{\partial x} = 1 - x_1$, at $x_1 = 0, 1$. The initial values are the constant functions $E(x,0) = 10^{-5}, T(x,0) = E(x,0)^{1/4}$, which is not an equilibrium of the PDEs because the nonlinear boundary condition at $x_1 = 1$ is not satisfied for E.

We consider for the space discretization two $n \times n$ grids with $n = 100$. The spectral radius are taken from [10, Section 4] and given by $\rho_D = 8.6\cdot10^4, \rho_R = 6\cdot10^6$. Similarly to the Brusselator problem considered in Section 4.1, the reaction is too stiff for a reasonable application of the standard methods ROCK2, RKC, and the partitioned method PRKC, and an implicit treatment of the reaction term is needed to avoid a severe step size restriction. We thus compare the PIROCK method only with the IRKC method. For the reference solution and plot of the numerical solution at final $T = 3$ in Fig. 12, we used PIROCK with the tolerance $tol = 10^{-8}$. We again compared this reference solution with the a reference solution given by IRKC (using the same tolerance) and checked that the significant digits where identical. The solution consists of a front moving from the left boundary (where the boundary condition is not satisfied) to the right boundary of the domain. It can be seen in Fig. 12 that the inhomogeneity located at the center of the domain, where the reaction is very stiff while the diffusion is smaller, greatly affects the shape of the solution (both E and T).

We take the initial step size $h = 10^{-5}$ for PIROCK, and compare the integrators PIROCK and IRKC in Fig. 11. Notice that for PIROCK with $tol = 10^{-2}$, the step size selection produced too large steps and the numerical solution became negative (the scalar $D_2 = kT^{5/2}$ is then no longer properly defined). We thus choose the largest tolerance for PIROCK as $tol = 10^{-2.5}$ and consider in Fig. 11 the tolerances $tol = 10^{-r/2}, r = 5\ldots9$ (PIROCK) and $tol = 10^{-r/2}, r = 2\ldots6$ (IRKC). It can be seen in Fig. 11comparing the L^2 error versus CPU time, that the PIROCK integrator is more efficient than RKC for the tolerances $tol = 10^{-r}, r = 2.5, 3, 3.5$. Notice that the spatial L^2-error for $n = 100$ is estimated as $3\cdot10^{-2}$ [10, Section 4.3.2] and that a uniform discretization in space is certainly not optimal (given the sharp front of the solution).

4.3. The 2D Brusselator problem with large advection

We consider the Brusselator problem in 2D where we add advection terms,

$$\begin{aligned}\frac{\partial u}{\partial t} &= v\Delta u + \mu U\cdot\nabla u + A + u^2 v - (B+1)u,\\ \frac{\partial v}{\partial t} &= v\Delta v + \mu V\cdot\nabla v + Bu - u^2 v,\end{aligned} \tag{54}$$

with $x \in (0,1)^2, t \in (0,1), A = 1.3, B = 1$,$U = (-0.5, 1)^T, V = (0.4, 0.7)^T$, with periodic boundary conditions and the initial condition (52). For the diffusion, we consider the parameter $v = 10^{-2}$. For the advection terms, we consider the values $\mu = 1$ and $\mu = 10^{-1}$, respectively. We discretize u, v in space with two $n \times n$ uniform meshes, where $n = 400$. For the integrators PRKC and PIROCK, we consider the partitioning where F_D corresponds to the discretized Laplacian $\Delta u, \Delta v$, and F_A corresponds to the other terms (advection and reaction). For $\mu = 1$, the solutions at point $x = (0,0)$ of PIROCK are plotted in Fig. 13 (left pictures) together with the corresponding variable stepsizes along the integration interval (right picture) for the tolerances $tol = 10^{-1}, 10^{-2}$. As predicted in Remark 3.4 (for the test PDE (36)), we observe that large steps of sizes up to $h \simeq 4\cdot10^{-2}$ are taken by the PIROCK method, whereas the PRKC method uses (nearly) constant stepsizes $h \simeq 1.6\cdot10^{-3}$ because of its stability constraint $h\rho_A \leqslant 1.7273$ (with $\rho_A \simeq 1040$). For the tolerances $tol = 10^{-r}, r = 2, \ldots, 5$, and the advection parameters $\mu = 1, 10^{-1}$, we compare in Fig. 14 the integrators RKC, ROCK2, PRKC, PIROCK. For the advection parameter $\mu = 10^{-1}$, it can be observed that both PRKC and PIROCK have a significantly reduced number of evaluations of F_A, corresponding to the advection and reaction, compared to RKC and ROCK2 (see the bottom right picture in Fig. 14). When the

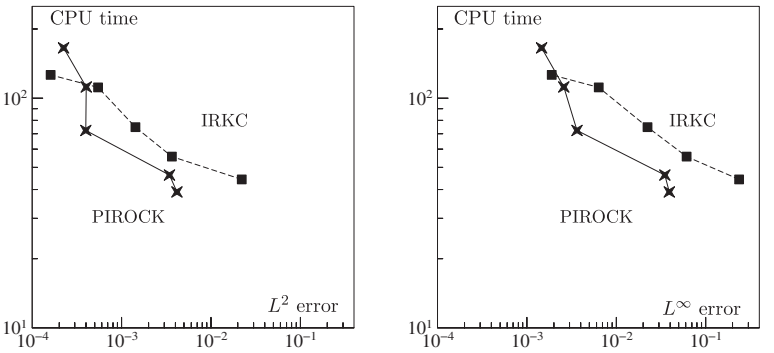

Fig. 11. Comparison of IRKC and PIROCK for the combustion problem (53) with a nonlinear diffusion and a stiff reaction. CPU time (seconds) versus L^2 and L^∞ errors for the tolerances $tol = 10^{-r/2}, r = 2 \dots 6$ (IRKC) and $tol = 10^{-r/2}, r = 5 \dots 9$ (PIROCK).

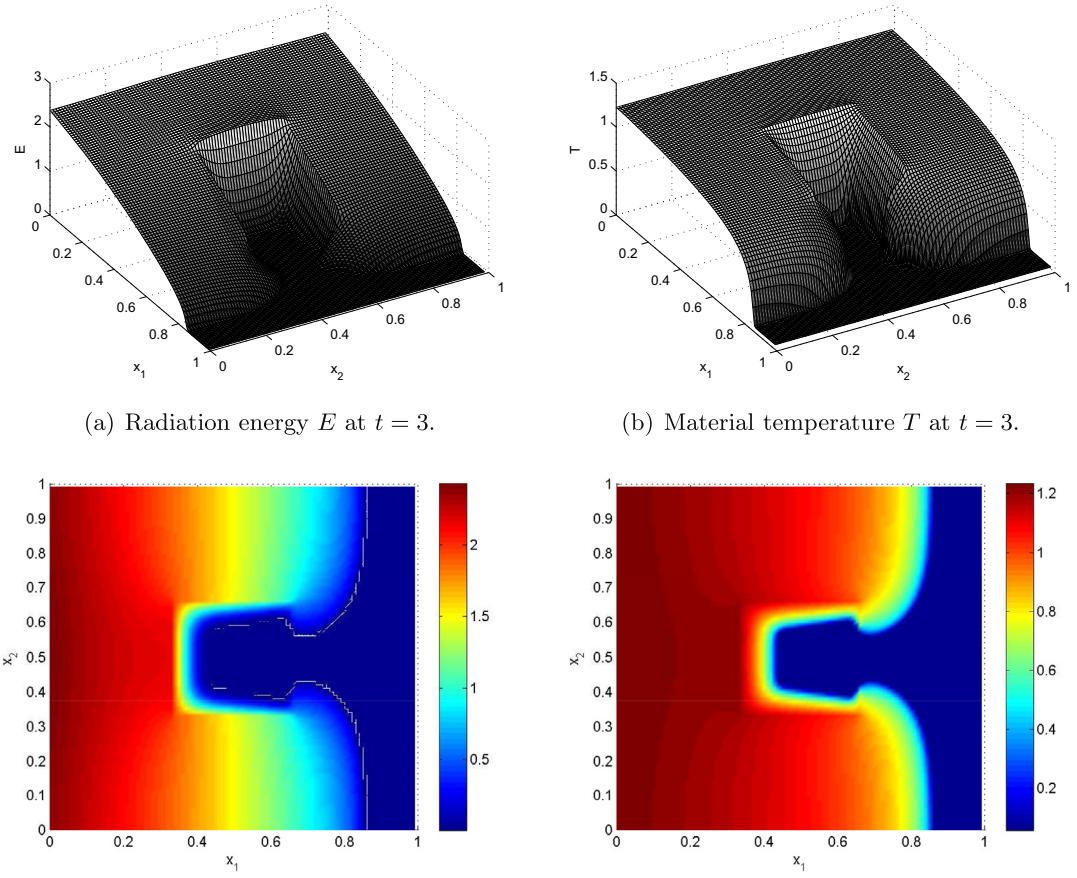

(a) Radiation energy E at $t = 3$.

(b) Material temperature T at $t = 3$.

(c) Radiation energy E at $t = 3$.

(d) Material temperature T at $t = 3$.

Fig. 12. Combustion problem with a nonlinear diffusion and a stiff reaction. Reference solution at $t = 3$. Spatial discretization: 100 $\times$ 100.

advection becomes large ($\mu = 1$), we observe that this is still the case for PIROCK but not for PRKC where the advection ellipse half-height is limited to $\simeq \sqrt{3}$ in the stability domain of the F_D–F_A coupling (notice that in this case, PRKC yields the same results for all considered tolerances and we obtain a single point in Fig. 14). We took the initial step size $h = 10^{-5}$ for all integrators, and used for the reference solution DOPRI5 [17] with tolerance $tol = 10^{-8}$. Notice that the integrator IRKC is less efficient than RKC for this problem as the reaction terms are non-stiff. Thus, we did not include the results with this integrator in our comparisons.

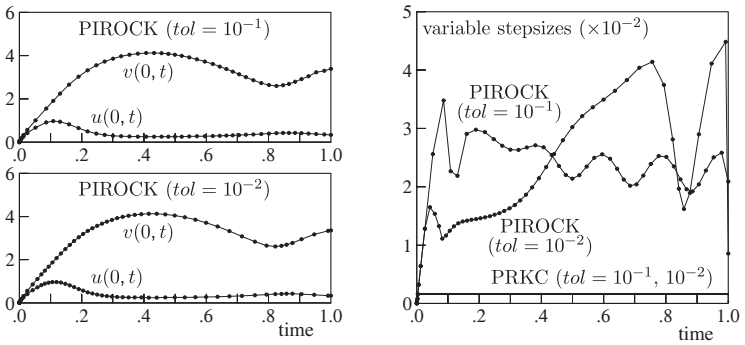

Fig. 13. Problem (54) with advection parameter $\mu = 1$. Left pictures: solutions with PIROCK at $x = (0,0)$ for the tolerances $tol = 10^{-1}, 10^{-2}$ as functions of time (the steps are plotted in bullet points). Right picture: corresponding variable stepsizes for PIROCK and PRKC (Initial stepsize is $h = 10^{-5}$).

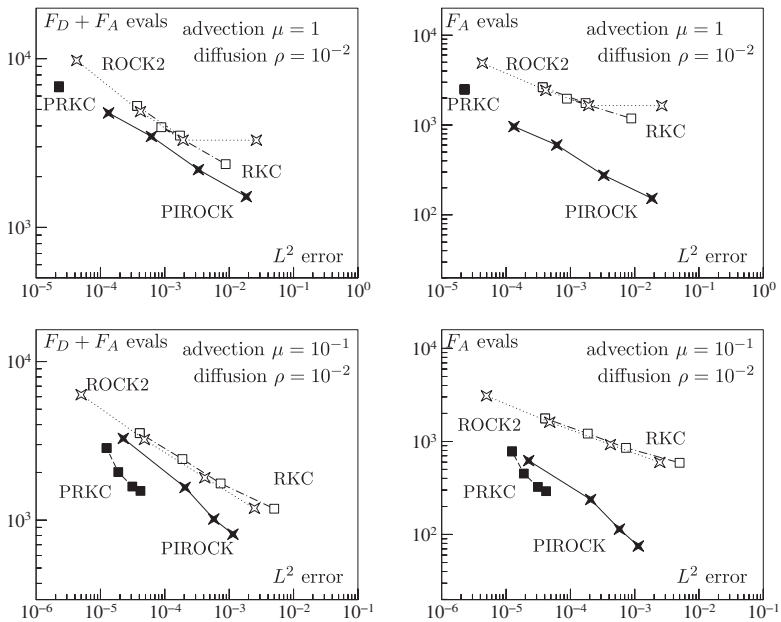

Fig. 14. Comparison of RKC (dashed-dotted lines), ROCK2 (dotted lines), PRKC (dashed lines), PIROCK (solid lines) for the 2D Brusselator problem with advection (54). Number of function evaluations versus L^2 errors for the tolerances $tol = 10^{-r}, r = 2 \dots 5$.

4.4. A 1D integro–differential equation

We consider the 1D integro–differential problem from [26] and considered in [12, Section 6.3], with an integral source term that is computationally expensive. It models the temperature profile of air near the ground,

$$\begin{aligned}
&\frac{\partial u}{\partial t}(x,t) = \frac{\partial u}{\partial x^2}(x,t) - \sigma \int_0^1 \frac{u(s,t)^4}{(1+|x-s|)^2} ds, \quad 0 \leqslant x,t \leqslant 1,\\
&u(x,0) = \cos^2(\pi x/2), \quad 0 \leqslant x \leqslant 1,\\
&u(0,t) = 1 - \sqrt{t}/2, \quad 0 \leqslant t \leqslant 1,\\
&u_x(1,t) = 0, \quad 0 \leqslant t \leqslant 1,
\end{aligned} \tag{55}$$

where $\sigma = 10^{-2}$. We discretize the space with a uniform grid with $n = 100$ mesh intervals. The integral is approximated by the second order trapezoidal rule $\int_0^1 f(s,u(s))ds \simeq n^{-1}(\sum_{i=1}^{n-1} f(x_i,u_i) + f(x_0,u_0)/2 + f(x_n,u_n)/2)$. We use for the Laplacian the standard second order central finite difference formula. The CPU time for all the integrators used in this experiments is very short and we rather present our comparisons in terms of function evaluations of the different components of the problem. In Table 2, we compare the integrators RKC, PRKC, ROCK2, PIROCK. For the integrators PRKC and PIROCK, we consider the partitioning where F_D corresponds to the discrete Laplacian, and F_A corresponds to the discretized integral source term. For RKC

Table 2
Comparison of RKC, ROCK, PRKC, PIROCK for the 1D integro–differential problem (55).

Method	tol	F_D evals	F_A evals	Steps(rej.)	s_{max}	L^2 errors	L^∞ errors
RKC	10^{-1}	857	857	10(2)	158	$1.0\cdot10^{-2}$	$1.8\cdot10^{-2}$
ROCK2	10^{-1}	617	617	10(0)	125	$1.7\cdot10^{-1}$	$7.3\cdot10^{-1}$
PRKC	10^{-1}	670	44	11(0)	139	$6.3\cdot10^{-3}$	$1.2\cdot10^{-2}$
PIROCK	10^{-1}	655	30	10(0)	114	$1.5\cdot10^{-1}$	$4.4\cdot10^{-1}$
RKC	10^{-2}	902	902	16(2)	139	$3.3\cdot10^{-3}$	$4.9\cdot10^{-3}$
ROCK2	10^{-2}	846	846	16(0)	87	$1.2\cdot10^{-2}$	$4.7\cdot10^{-2}$
PRKC	10^{-2}	991	76	19(0)	80	$5.3\cdot10^{-4}$	$7.4\cdot10^{-4}$
PIROCK	10^{-2}	898	48	16(0)	80	$1.9\cdot10^{-2}$	$1.3\cdot10^{-1}$
RKC	10^{-3}	1026	1026	25(3)	96	$7.6\cdot10^{-4}$	$1.0\cdot10^{-3}$
ROCK2	10^{-3}	1245	1245	33(0)	63	$1.5\cdot10^{-3}$	$8.3\cdot10^{-3}$
PRKC	10^{-3}	1760	204	51(0)	44	$4.8\cdot10^{-5}$	$7.5\cdot10^{-5}$
PIROCK	10^{-3}	1426	105	35(0)	58	$1.9\cdot10^{-3}$	$1.3\cdot10^{-2}$
RKC	10^{-4}	1390	1390	45(2)	70	$1.7\cdot10^{-4}$	$2.4\cdot10^{-4}$
ROCK2	10^{-4}	1923	1923	83(2)	41	$1.3\cdot10^{-4}$	$7.7\cdot10^{-4}$
PRKC	10^{-4}	3467	700	175(5)	26	$5.1\cdot10^{-6}$	$1.0\cdot10^{-5}$
PIROCK	10^{-4}	2973	366	134(12)	41	$1.6\cdot10^{-4}$	$1.3\cdot10^{-3}$

and ROCK2, we consider the single vector field $F = F_D + F_A$. We take the initial step size $h = 10^{-3}$ and we consider the tolerances $tol = 10^{-r}, r = 1,2,3,4$, respectively. We report the L^2 and L^∞ errors compared to a reference solution computed with DOPRI5 with tolerance $tol = 10^{-8}$. Notice that for large n, the evaluation of F_D has complexity $\mathcal{O}(n)$, while the evaluation of F_A has complexity $\mathcal{O}(n^2)$ and thus dominates the cost. Compared to RKC and ROCK2, we observe that for all considered tolerances, the partitioning F_D–F_A in PRKC and PIROCK permits to reduce by one order of magnitude the number of function evaluations of the most costly integral term F_A, as illustrated in Table 2. We again emphasize that IRKC presents no advantage compared to RKC for this problem.

4.5. A 2D brusselator with non-symmetric diffusion, advection, a highly stiff reaction, and stiff Itô stochastic noise

To illustrate the versatility of the proposed PIROCK integrator, we consider the Brusselator problem with simultaneously all the difficulties of a non-symmetric diffusion operator, a stiff reaction, advection, and a two-dimensional stiff Itô stochastic noise, defined as

$$\begin{aligned}\frac{\partial u}{\partial t} &= v\Delta u + v/2 \quad \Delta v + \mu U\cdot\nabla u + \big(A + u^2 v - (B+1)u\big) + (\sigma_{11} + \sigma_{12}u)\dot{W}_1,\\ \frac{\partial v}{\partial t} &= -v/2\,\Delta u + v\Delta v + (\mu V\cdot\nabla v + f) + \big(Bu - u^2 v\big) + (\sigma_{21} + \sigma_{22}uv)\dot{W}_2.\end{aligned} \tag{56}$$

For this problem we thus have to open all the blades of the "swiss-knife". For the diffusion and advection parameters, we take $v = 0.1, \mu = 0.1, U = (-0.5,1)^T, V = (0.4,0.7)^T$. We also consider a stiff reaction with parameters $A = 1.3, B = 10^7$, and with stiff noise parameters $\sigma_{11} = 3, \sigma_{12} = 4.4\cdot10^3, \sigma_{21} = 0.5, \sigma_{22} = 1$. Notice that since $-B + \sigma_{21}^2/2 < 0$, the reaction-noise system can be shown to be mean–square stable. We also consider an inhomogenity defined as $f(x) = 5$ if $(x_1 - 0.3)^2 + (x_2 - 0.6)^2 \leqslant 0.3^2$, and $f(x) = 0$ else. We consider a space discretization with two 200×200 meshes and consider the constant time step size $h = 10^{-2}$ on the time interval $(0,1)$. The number of stages used at each step to treat the diffusion is $s_{max} = 28$. We plot in Fig. 15 one realization of the problem (56). In picture 15(a), we plot the solutions

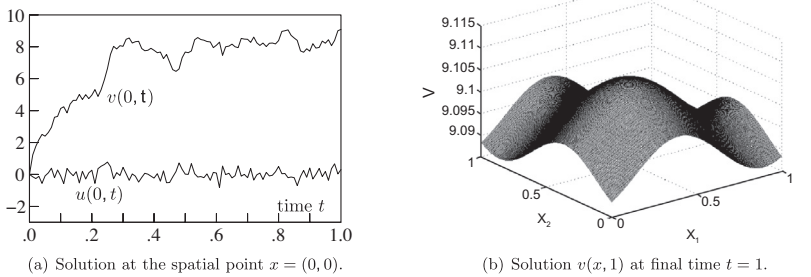

(a) Solution at the spatial point $x = (0,0)$.

(b) Solution $v(x,1)$ at final time $t = 1$.

Fig. 15. Non-symmetric diffusion–advection–reaction-noise problem (56). Space discretization: two 200×200 meshes. Constant step size $h = 10^{-2}$.

$u(x,t)$, $v(x,t)$ as a function of time t for $x=(0,0)$ fixed, while in picture 15(b), we plot the solution $v(x,t)$ at final time $t=1$ as a function of the spatial variable $x=(x_1,x_2)$. It can be seen that the solution oscillates stochastically in time, while it remains smooth in space. Notice that for the standard Euler–Maruyama method, the step size restriction for mean-square stability can be estimated as $h \leqslant 0.64 \cdot 10^{-8}$, which makes this method of no practical use for this problem.

Source code for PIROCK and some examples are available at `http://anmc.epfl.ch`

Any feedback for this code is welcome.

Acknowledgements

The authors are grateful to Ernst Hairer and Christophe Zbinden for helpful comments on an earlier version of the manuscript, and for providing the FORTRAN codes and drivers of IRKC and PRKC. The research of A. A. is partially supported by the Swiss National Foundation Grant 200021_140692.

References

[1] E. Hairer, G. Wanner, Solving Ordinary Differential Equations II. Stiff and Differential–Algebraic Problems, Springer Verlag, Berlin and Heidelberg, 1996.
[2] W. Hundsdorfer, J. Verwer, Numerical solution of time-dependent advection–diffusion–reaction equations, Springer Series in Computational Mathematics, vol. 33, Springer-Verlag, Berlin, 2003.
[3] V. Lebedev, Explicit difference schemes with time-variable steps for solving stiff systems of equations, Sov. J. Numer. Anal. Math. Model. 4 (2) (1989) 111–135.
[4] P. Van der Houwen, B. Sommeijer, On the internal stage Runge–Kutta methods for large m-values, Z. Angew. Math. Mech. 60 (1980) 479–485.
[5] A. Abdulle, A. Medovikov, Second order Chebyshev methods based on orthogonal polynomials, Numer. Math. 90 (1) (2001) 1–18.
[6] A. Abdulle, Fourth order Chebyshev methods with recurrence relation, SIAM J. Sci. Comput. 23 (6) (2002) 2041–2054.
[7] J.G. Verwer, B.P. Sommeijer, W. Hundsdorfer, RKC time-stepping for advection–diffusion–reaction problems, J. Comput. Phys. 201 (1) (2004) 61–79.
[8] A. Abdulle, Chebyshev methods based on orthogonal polynomials, Ph.D. thesis, University of Geneva, Department of Mathematics, University of Geneva, 2001.
[9] M. Duarte, M. Massota, S. Descombes, C. Tenaudc, T. Dumont, V. Louvet, F. Laurent, New resolution strategy for multi-scale reaction waves using time operator splitting, space adaptive multiresolution and dedicated high order implicit/explicit time integrators, SIAM J. Sci. Comput. 34 (1) (2012) 76–104.
[10] J.G. Verwer, B.P. Sommeijer, An implicit–explicit Runge–Kutta–Chebyshev scheme for diffusion–reaction equations, SIAM J. Sci. Comput. 25 (5) (2004) 1824–1835.
[11] B.P. Sommeijer, J.G. Verwer, On stabilized integration for time-dependent PDEs, J. Comput. Phys. 224 (1) (2007) 3–16.
[12] C.J. Zbinden, Partitioned Runge–Kutta–Chebyshev methods for diffusion–advection–reaction problems, SIAM J. Sci. Comput. 33 (4) (2011) 1707–1725.
[13] A. Abdulle, S. Cirilli, S-ROCK: Chebyshev methods for stiff stochastic differential equations, SIAM J. Sci. Comput. 30 (2) (2008) 997–1014.
[14] A. Abdulle, T. Li, *S*-ROCK methods for stiff Ito SDEs, Commun. Math. Sci. 6 (4) (2008) 845–868.
[15] A. Abdulle, G. Vilmart, K. Zygalakis, Mean–square *A*-stable diagonally drift-implicit integrators of weak second order for stiff Itô stochastic differential equations, EPFL MATHICSE Research Report No. 35.2012.
[16] A. Abdulle, G. Vilmart, K. Zygalakis, Weak second order explicit stabilized methods for stiff stochastic differential equations, EPFL MATHICSE Research Report No. 05.2012, submitted for publication.
[17] E. Hairer, S. Nørsett, G. Wanner, Solving ordinary differential equations I. Nonstiff problems, Springer Verlag Series in Comput. Math., vol. 8, Berlin, 1993.
[18] K. Burrage, W.H. Hundsdorfer, J.G. Verwer, A study of *B*-convergence of Runge–Kutta methods, Computing 36 (1986) 17–34.
[19] J. Verwer, W. Hundsdorfer, B. Sommeijer, Convergence properties of the Runge–Kutta–Chebyshev method, Numer. Math. 57 (1990) 157–178.
[20] A. Abdulle, G. Vilmart, Coupling heterogeneous multiscale FEM with Runge–Kutta methods for parabolic homogenization problems: a fully discrete space–time analysis, Math. Models Methods Appl. Sci. 22 (6) (2012) 1250002/1–1250002/40.
[21] Y. Saito, T. Mitsui, Stability analysis of numerical schemes for stochastic differential equations, SIAM J. Numer. Anal. 33 (1996) 2254–2267.
[22] D. Higham, *A*-stability and stochastic stability mean–square stability, BIT 40 (2000) 404–409.
[23] K. Burrage, P. Burrage, T. Tian, Numerical methods for strong solutions of stochastic differential equations: an overview, Proc. R. Soc. Lond. Ser. A Math. Phys. Eng. Sci. 460 (2041) (2004) 373–402.
[24] A. Tocino, Mean–square stability of second-order Runge–Kutta methods for stochastic differential equations, J. Comput. Appl. Math. 175 (2) (2005) 355–367.
[25] V. Mousseau, D. Knoll, W. Rider, Physics-based preconditioning and the Newton–Krylov method for non-equilibrium radiation diffusion, J. Comput. Phys. 160 (2000) 743–765.
[26] A.S. Vasudeva Murthy, J.G. Verwer, Solving parabolic integro–differential equations by an explicit integration method, J. Comput. Appl. Math. 39 (1992) 121–132.